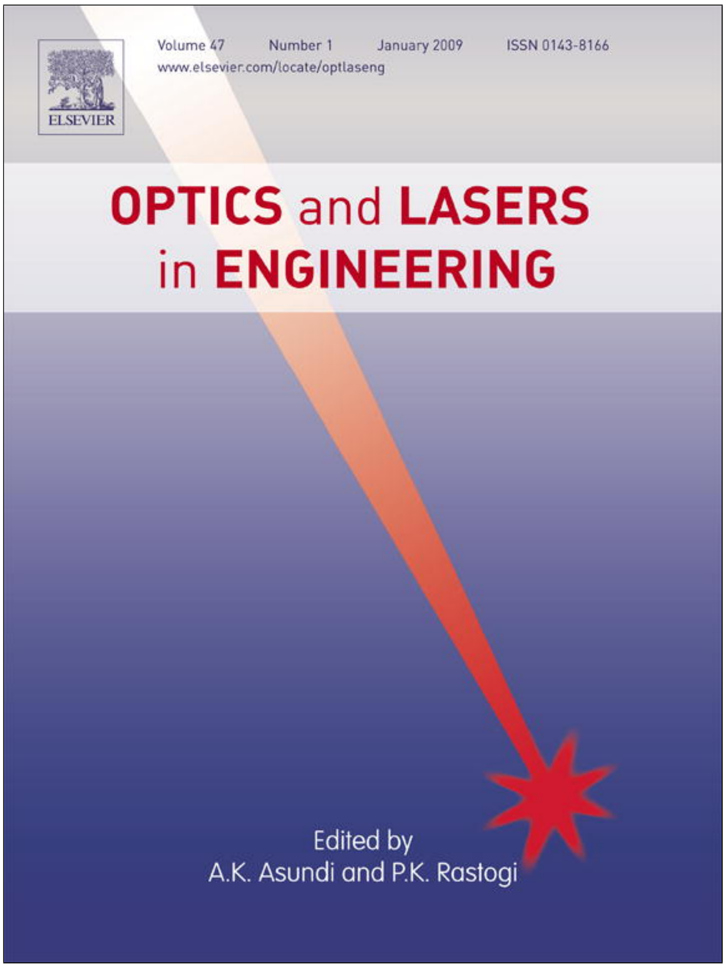
Volume 47 Number 1 January 2009 ISSN 0143-8166
www.elsevier.com/locate/optlaseng
ELSEVIER
OPTICS and LASERS in ENGINEERING
Edited by
A.K. Asundi and P.K. Rastogi

Optics and Lasers in Engineering 47 (2009) 31–38

Contents lists available at ScienceDirect

Optics and Lasers in Engineering

journal homepage: www.elsevier.com/locate/optlaseng

Spatial anisotropy of linear electro-optic effect in crystal materials: I—Experimental determination of electro-optic tensor in $LiNbO_3$ by means of interferometric technique

A.S. Andrushchak [a], B.G. Mytsyk [b], N.M. Demyanyshyn [b], M.V. Kaidan [a], O.V. Yurkevych [a], I.M. Solskii [c], A.V. Kityk [d,*], W. Schranz [e]

[a] Lviv Polytechnic National University, 12 S. Bandery Str., 79013 Lviv, Ukraine
[b] Karpenko Physico-Mechanical Institute, 5 Naukova Str., 79601 Lviv, Ukraine
[c] Scientific Research Company "Carat", 202 Stryjska Str., 79031 Lviv, Ukraine
[d] Department of Electrical Engineering, Institute for Computer Science, Czestochowa University of Technology, Al. Armii Krajowej 17, PL-42200 Czestochowa, Poland
[e] Faculty of Physics, University of Vienna, Boltzmanngasse 5, A-1090 Vienna, Austria

ARTICLE INFO

Article history:
Received 9 May 2008
Received in revised form
12 August 2008
Accepted 14 August 2008
Available online 2 October 2008

Keywords:
Linear electro-optic effect
Interferometry
Triclinic symmetry
Pure and MgO-doped lithium niobate crystals
Electro-optic coefficients

ABSTRACT

The paper presents a technique suitable for the determination of linear electro-optic effect (LEOE) tensor components in crystal materials of any symmetry. The method is based on the Michelson interferometer, where the sample being studied is set into one of its arms to measure the electro-induced changes of the optical path. We describe in detail the sample geometries that are needed to determine a complete set of the LEOE tensor components and derive the corresponding equations. The experimental technique has been tested and verified on lithium niobate crystals as well as applied to MgO-doped $LiNbO_3$ crystals to study their electro-optic properties. The developed method can be useful for optical engineering, which deals with new materials being used in design or production of devices, such as, e.g., modulators or deflectors.

1. Introduction

Nowadays, linear electro-optic effect (LEOE) has found a large number of practical applications, especially in solid-state electronic and optoelectronic devices [1,2]. A growing interest on these studies is due to recent developments in fields of crystals growth and technology [3–5], leading to the appearance of new efficient electro-optic crystals [6–8]. The structure of such materials is frequently described by low-symmetry groups and it reveals substantial anisotropy of optical properties. Hence, the application of electro-optic crystals, usually as media for electro-optic modulators or deflectors, requires knowledge of the spatial anisotropy of their physical properties. The main problems rise here in regard to the optimization of electro-optic interaction geometry, which makes it possible to use only these materials with maximal efficiency. Such problems may be solved in terms of indicative surfaces, which may be calculated only if a complete set of LEOE tensor components is known. The procedure given here is then similar to the recently reported one for the case of piezo-optic effect [9–11].

Methods suitable for determination of a complete set of LEOE for an arbitrary crystal symmetry (in particular for low-symmetry crystals) have never been reported, although experimental measurements of LEOE for high-symmetry optical materials (such as, e.g., optically uniaxial or cubic crystals) have been performed by a large number of research groups (see, e.g., Refs. [12,13] and references therein). Sonin and Vasilevskaya [14] report the equations that describe changes in the optical indicatrix under an applied electric field. However, it does not consider the case of triclinic symmetry. Also the equations presented there are of low practical importance since they cannot be directly used for the determination of LEOE coefficients.

In the present paper we describe the technique suitable for determination of LEOE tensor components in a crystal material of any symmetry. The method is based on the Michelson interferometer. We describe here in detail the sample geometries that are needed to determine a complete set of the LEOE tensor components and we derive the corresponding equations. The experimental technique will then be tested on lithium niobate crystals and will also be applied to new crystals of MgO-doped

* Corresponding author.
E-mail address: andriy.kityk@univie.ac.at (A.V. Kityk).

0143-8166/$ - see front matter © 2008 Elsevier Ltd. All rights reserved.
doi:10.1016/j.optlaseng.2008.08.005

$LiNbO_3$ to study their electro-optic properties. $LiNbO_3$:MgO crystals have a radiation resistance about four times higher than that of pure $LiNbO_3$ [15]. Due to this reason such materials are promising for numerous practical applications since they provide the best parameter stability with powerful laser radiation. In a following paper [16] we report on the indicative surfaces of these crystals, which give a direct characterization of spatial anisotropy analysis of the LEOE and may thus be used for selection of an appropriate sample geometry. Taken together, these articles form a guide for developing and designing highly efficient electro-optic cells made of crystal materials.

2. Experimental technique and description of the method

The experimental determination of LEOE coefficients is based on measurements of electro-induced changes of optical path in crystal materials, where interferometric techniques are usually accepted as the most precise and appropriate [12]. Fig. 1 shows the experimental setup, which is based on the Michelson interferometer. The sample being measured is set into one arm of the interferometer. Accordingly, the optical path introduced by the sample is $\Delta_{ikl} = 2(n_i - n_p)t_k$, where n_i and n_p are the refractive indices of a sample material and surrounding media ($n_p = 1$ in the case of air), respectively, and t_k is the sample length in the direction of light propagation **k**. Hence, the induced changes of the optical path $\delta\Delta_{ikl}$ under the applied electric field $E_l = U/l$ (U is the voltage applied to the sample of a thickness l) is defined by the equation

$$\begin{aligned}\delta\Delta_{ikl} &= 2(t_k\,\delta n_i + (n_i - 1)\delta t_k)\\ &= -r_{il}n_i^3E_lt_k + 2(n_i - 1)d_{lk}E_lt_k, \qquad (1)\end{aligned}$$

where the subscript indices i (direction of light polarization), k (direction of light propagation) and l (direction of applied electric field) correspond to the principal axes of the rectangular sample, d_{lk} and r_{il} are the tensor components of inverse piezoelectric effect and LEOE in matrix representation [12], respectively. The electro-induced changes of the optical path lead to a shift of the interference fringe in the output of interferometer and accordingly change the light intensity on the photodiode PD [see Fig. 1]. For practical reasons it is convenient to set the interference shift $\delta\Delta_{ikl} = n\lambda/2$ (where $n = 1, 2, \ldots$) by adjusting the applied dc-voltage to the sample. If $n = 1$ the corresponding voltage difference is frequently called the half-wave voltage $U^{\lambda/2}$. In such cases the interference minimum is replaced by the interference maximum or vice versa, which may be easily detected. One must emphasize that the first term of Eq. (1) describes the optical path changes due to the electro-optic effect, which is directly related to the changes of refractive indices $\delta n_i = -\delta a_i/(2a_i^{3/2}) = -r_{il}E_ln_i^3/2$ [δa_i are the changes of relevant optical polarization constants a_i]. The second term corresponds to the optical path changes due to the inverse piezoelectric effect, i.e. it is caused by changes of the sample length in the direction of light propagation under the applied electric field E_l ($\delta t_k = d_{lk}E_lt_k$). Unit vectors of the triad **i**, **k** and **l** are perpendicular to each other only for transverse LEOE. In the case of longitudinal LEOE the unit vectors **i** and **l** are parallel. The sign as well as absolute magnitudes of LEOE coefficients may be unambiguously determined by applying the following three rules:

- The sign of $\delta\Delta_{ikl}$ is accepted as positive if a rise of positive electric field E_l leads to an increase of the optical path $\delta\Delta_{ikl}$.
- The positive directions regarding the crystallophysical axes are set according to the IRE standard [17] with additions for photoelasticity given in our work [18].
- The positive direction of the electric field E_l is chosen as in electrodynamics (i.e. from the positive electrode to the negative electrode). In addition, the direction of electric field vector must coincide with the positive direction of the corresponding crystallophysical axis.

It should be stressed here that in low-symmetry crystals the crystallographic (X, Y, Z) and the crystallophysical (X_1, X_2, X_3) systems for different effects frequently do not coincide. Therefore, by using, e.g., known magnitudes of the piezoelectric tensor components d_{lk} one must transform them in accordance with the crystallooptic system, i.e. with the principal axes of the optical indicatrix.

3. Derivation of basic equations

In order to determine a complete set of LEOE tensor components for crystals of the lowest triclinic symmetry (point groups 1 or $\bar{1}$) one must prepare four samples: one sample of a rectangular shape with faces perpendicular to the principal crystallooptic axes [hereafter referred to as direct cut (DC) sample] as shown in Fig. 2(a), and three samples of rectangular shape but turned around the X_1 (X or 1) [Fig. 2(b)], X_2 (Y or 2) [Fig. 2(c)] or X_3 (Z or 3) [Fig. 2(d)] axis by the angle of 45° [hereafter referred to as X_1/45°- , X_2/45°- or X_3/45°-cut samples]. The DC-sample is needed to determine the nine tensor components r_{il} (i, $l = 1, 2, 3$) describing the deformation of the optical indicatrix, whereas 45° cuts are used to determine remaining nine tensor components r_{il} ($i = 4, 5, 6$, $l = 1, 2, 3$), which are responsible for an optical indicatrix rotation under the applied electric field E_l.

Let us describe in detail how to determine a complete set of LEOE coefficients for triclinic crystals. It is important here to follow a sequence of sample geometries being measured

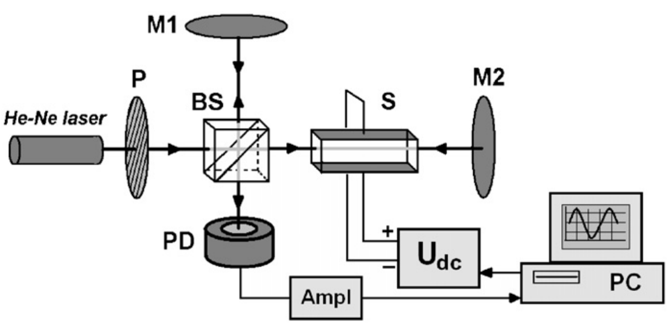

Fig. 1. Experimental setup for electro-optic measurements: BS is the beam splitter, M1 and M2 are the mirrors, P is the polarizer, U_{dc} is the high dc-voltage source controlled by the personal computer (PC), S is the rectangular sample with deposited gold electrodes, PD is the photodiode and Ampl is the amplifier.

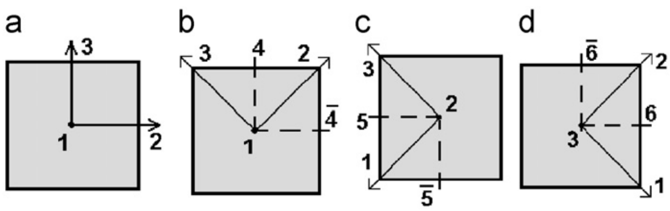

Fig. 2. Four possible rectangular sample orientations as suggested for the electro-optic measurements: (a) DC-sample, (b) X_1/45°-cut sample, (c) X_2/45°-cut sample and (d) X_3/45°-cut sample. The presented set of samples is the minimally required one to determine a complete set of LEOE tensor components in triclinic crystals. For crystals of higher symmetry the required number of various samples is reduced.

as presented below. In particular, the nine measurements on DC-samples should be done first. This indeed requires preparation of three samples, with the electrodes deposited on the faces perpendicular to X_1-, X_2- or X_3-axis. The LEOE coefficients r_{il} $(i, l = 1, 2, 3)$ can then be calculated according to the expression that directly follows from Eq. (1):

$$r_{il} = -n_i^{-3}\frac{\delta\Delta_{ikl}}{t_k E_l} + 2n_i^{-3} d_{lk}(n_i - 1). \tag{2}$$

It must be mentioned that each of these samples is suitable for the determination of only three LEOE coefficients. In uniaxial crystals that are characterized by point groups of symmetry such as 62m, 6, 32 or 3, Eq. (2) reduces to a simpler form for the LEOE coefficient r_{11}. A similar remark can also be addressed regarding the LEOE coefficient r_{22} for crystals described by point groups of symmetry 6, 3m or 3. We have here in mind the sample geometries $i = 1$, $k = 3$, $l = 1$ (as for r_{11}) or $i = 2$, $k = 3$, $l = 2$ (as for r_{22}) for which corresponding coefficients of inverse piezoelectricity are equal to zero. Thus Eq. (2) in each of these cases takes the following form:

$$r_{11} = -n_1^{-3}\frac{\delta\Delta_{131}}{t_3 E_1}, \quad r_{22} = -n_2^{-3}\frac{\delta\Delta_{232}}{t_3 E_2}. \tag{3}$$

To determine the remaining nine LEOE coefficients r_{il} $(i = 4, 5, 6, l = 1, 2, 3)$ one should prepare $X_1/45°$-, $X_2/45°$- and $X_3/45°$-cut samples. In particular, the effective LEOE coefficients r_{41}, r_{52} or r_{63} may be determined on the samples with electrodes deposited on the faces perpendicular to X_1-, X_2- or X_3-axis, respectively. For each of these sample geometries one can directly measure the induced changes of the optical path:

$$\delta\Delta'_{ikl} = -r'_{il} n'^3_i E_l t_k + 2d'_{lk}(n'_i - 1)E_l t_k, \tag{4}$$

which are expressed through the so-called effective magnitudes r'_{il} and d'_{lk} in the rotated (by a 45°) coordinate system. The latter ones can be transformed to required magnitudes r_{il} and d_{lk} (i.e. in the basic coordinate system) applying straightforward tensor transformations:

$$r'_{il} \equiv r'_{jpl} = \alpha_{jf}\alpha_{pg}\alpha_{lq} r_{fgq}, \quad d'_{lk} \equiv d'_{ljp} = \alpha_{lq}\alpha_{jf}\alpha_{pg} d_{qfg}, \tag{5}$$

where r_{jpl} and d_{ljp} are the tensor components of the linear electro-optic and inverse piezoelectric effects, respectively. Here, according to [12], the indices i and k are given in Voight notation, i.e. $11 \leftrightarrow 1$, $22 \leftrightarrow 2$, $33 \leftrightarrow 3$, $23 \leftrightarrow 4$, $13 \leftrightarrow 5$, $12 \leftrightarrow 6$; $\alpha_{lq}, \alpha_{kf}, \alpha_{ig}, \ldots$ are the directional cosines between the axes of the basic and rotated Cartesian coordinate systems $(f, g, q = 1, 2, 3)$. Similarly, the refractive index n'_i is expressed through the second-rank tensor of optical polarization constants a'_i and the refractive index in principal crystallophysical coordinate system n_g. Thereby

$$n'_i = 1\Big/\sqrt{a'_i} = 1\Big/\sqrt{\alpha_{ig}^2 a_g} = 1\Big/\sqrt{\alpha_{ig}^2 n_g^{-2}}. \tag{6}$$

To determine, e.g., the LEOE coefficients r_{41}, one must use $X_1/45°$-cut sample [Fig. 2(b)] with the deposited electrodes perpendicular to the X_1-axis. Actually two sample geometries can be used: $i = 4$, $k = \bar{4}$, $l = 1$ (called hereafter as a direct geometry) and $i = \bar{4}$, $k = 4$, $l = 1$ (called hereafter as a symmetric geometry), where by index 4 and $\bar{4}$ we denote the diagonal direction between the positive directions of axes X_2 and X_3 and the direction orthogonal to it, respectively [see Fig. 2(b)]. In this case the directional cosines are $\alpha_{i1} = 0$, $\alpha_{i2} = \sqrt{2}/2$, $\alpha_{i3} = \pm\sqrt{2}/2$, $\alpha_{k1} = 0$, $\alpha_{k2} = \sqrt{2}/2$, $\alpha_{k3} = \mp\sqrt{2}/2$, $\alpha_{l1} = 1$, $\alpha_{l2} = 0$, $\alpha_{l3} = 0$, where the lower sign corresponds to the case of the symmetric geometry. Inserting these values into Eqs. (5) and (6) one obtains the expressions for the effective magnitudes r'_{il}, d'_{kl} and n'_i:

$$\begin{aligned} r'_{41} &= \tfrac{1}{2}(r_{21} + r_{31} \pm 2r_{41}), \\ d'_{14} &= \tfrac{1}{2}(d_{12} + d_{13} \mp d_{14}), \\ n_4 &= \sqrt{2}/\sqrt{n_2^{-2} + n_3^{-2}}, \end{aligned} \tag{7}$$

which by means of Eq. (4) can be transformed to the required expressions for the LEOE coefficient r_{41} in the basic coordinate system:

$$\begin{aligned} r_{41} = &-n_4^{-3}\frac{\delta\Delta_{4\bar{4}1}}{t_{\bar{4}} E_1} + n_4^{-3}(n_4 - 1)(d_{12} + d_{13} - d_{14}) \\ &- \frac{1}{2}(r_{21} + r_{31}), \end{aligned} \tag{8a}$$

$$\begin{aligned} r_{41} = &\, n_4^{-3}\frac{\delta\Delta_{\bar{4}41}}{t_4 E_1} - n_4^{-3}(n_4 - 1)(d_{12} + d_{13} + d_{14}) \\ &+ \frac{1}{2}(r_{21} + r_{31}). \end{aligned} \tag{8b}$$

Here Eqs. (8a) and (8b) correspond to chosen sample geometries (direct and symmetric one, respectively). One should keep in mind that the sign of r_{41} as well as d_{14} is directly bonded to the chosen crystallophysical coordinate system, which is assumed to be set up according to [17,18]. By adding Eqs. (8a) and (8b) one eliminates the tensor components r_{21}, r_{31}, d_{12} and d_{13} leading thus to a much simplified expression (T.1) [see Table 1] suitable for a more accurate evaluation of the LEOE coefficient r_{41}. In a similar way we have derived corresponding equations for the LEOE coefficients r_{52} and r_{63}. They are presented in Table 1.

The LEOE coefficients r_{61}, r_{62}, r_{53}, r_{51}, r_{42} and r_{43} can be determined by using the samples of 45°-cuts [see Figs. 2(b)–(d)]. Measurements are performed in each case on the pair of samples with electrodes deposited on faces that are perpendicular to the axes (6 and $\bar{6}$), (5 and $\bar{5}$) or (4 and $\bar{4}$). Accordingly, the direct conditions for the $X_1/45°$-cut sample [Fig. 2(b)] are $i = 4$, $k = \bar{4}$, $l = 4$ whereas for the asymmetric ones they are $i = \bar{4}$, $k = 4$, $l = \bar{4}$. In this case the directional cosines are $\alpha_{i1} = 0$, $\alpha_{i2} = \sqrt{2}/2$, $\alpha_{i3} = \pm\sqrt{2}/2$ as for the direction of light polarization **i**, $\alpha_{k1} = 0$, $\alpha_{k2} = \sqrt{2}/2$, $\alpha_{k3} = \mp\sqrt{2}/2$ as for the direction of light propagation **k** and $\alpha_{l1} = 0$, $\alpha_{l2} = \sqrt{2}/2$, $\alpha_{l3} = \sqrt{2}/2$ as for the direction of the applied electric field **l**. Then the effective LEOE coefficients for the triclinic symmetry are described by the following equations:

$$\begin{aligned} r'_{44} &= \frac{\sqrt{2}}{4}(r_{22} \pm r_{23} + r_{32} \pm r_{33} \pm 2r_{42} + 2r_{43}), \\ d'_{4\bar{4}} &= \frac{\sqrt{2}}{4}(d_{22} + d_{23} \pm d_{32} \pm d_{33} \mp d_{24} - d_{34}), \\ n_4 &= \sqrt{2}/\sqrt{n_2^{-2} + n_3^{-2}}. \end{aligned} \tag{9}$$

By inserting Eq. (9) into Eq. (4) one obtains two relations that correspond to the direct or symmetric conditions. Further mutual adding or subtracting of these equations lead to two new relations suitable for determination of the LEOE coefficients r_{42}, r_{43} [see Table 1, Eqs. (T.4) and (T.5)]. These equations as well as the relations for determination of the LEOE coefficients r_{61}, r_{62}, r_{53}, r_{51} [Eqs. (T.6)–(T.9), Table 1] are subjected to a further considerable reduction if one deals with crystals of higher symmetry. In special cases the LEOE coefficients r_{61}, r_{62}, r_{53}, r_{51}, r_{42}, r_{43} can be determined using only the direct conditions in experimental measurements. The corresponding equations for such cases are presented in Table 2. In addition, the same samples can also be used to determine the principal diagonal LEOE coefficients, i.e. r_{11}, r_{22} or r_{33} for which $i = l$ and $k = 4(\bar{4})$, $5(\bar{5})$ or $6(\bar{6})$, respectively. Sometimes such measurements appear to be useful or even quite desirable, especially in the case when an independent verification of the results obtained on the DCs is needed [see Table 3].

Table 1
Relations for determination of the non-principal LEOE tensor components r_{il} in crystals of triclinic symmetry by means of Michelson interferometer

Sample	Relation	Equation
Fig. 2(b)	$r_{41}=-\frac{1}{2}n_4^{-3}\left(\frac{\delta\Delta_{4\bar{4}1}}{t_{\bar{4}}E_1}-\frac{\delta\Delta_{\bar{4}41}}{t_4E_1}\right)-n_4^{-3}(n_4-1)d_{14}$	T.1
Fig. 2(c)	$r_{52}=-\frac{1}{2}n_5^{-3}\left(\frac{\delta\Delta_{5\bar{5}2}}{t_{\bar{5}}E_2}-\frac{\delta\Delta_{\bar{5}52}}{t_5E_2}\right)-n_5^{-3}(n_5-1)d_{25}$	T.2
Fig. 2(d)	$r_{63}=-\frac{1}{2}n_6^{-3}\left(\frac{\delta\Delta_{6\bar{6}3}}{t_{\bar{6}}E_3}-\frac{\delta\Delta_{\bar{6}63}}{t_6E_3}\right)-n_6^{-3}(n_6-1)d_{36}$	T.3
Fig. 2(b)	$r_{43}=-\frac{\sqrt{2}}{2}n_4^{-3}\left(\frac{\delta\Delta_{4\bar{4}4}}{t_{\bar{4}}E_4}+\frac{\delta\Delta_{\bar{4}4\bar{4}}}{t_4E_{\bar{4}}}\right)+n_4^{-3}(n_4-1)(d_{22}+d_{23}-d_{34})-(r_{22}+r_{32})/2$	T.4
	$r_{42}=-\frac{\sqrt{2}}{2}n_4^{-3}\left(\frac{\delta\Delta_{4\bar{4}4}}{t_{\bar{4}}E_4}-\frac{\delta\Delta_{\bar{4}4\bar{4}}}{t_4E_{\bar{4}}}\right)+n_4^{-3}(n_4-1)(d_{32}+d_{33}-d_{24})-(r_{23}+r_{33})/2$	T.5
Fig. 2(c)	$r_{51}=-\frac{\sqrt{2}}{2}n_5^{-3}\left(\frac{\delta\Delta_{5\bar{5}5}}{t_{\bar{5}}E_5}-\frac{\delta\Delta_{\bar{5}5\bar{5}}}{t_5E_{\bar{5}}}\right)+n_5^{-3}(n_5-1)(d_{31}+d_{33}-d_{15})-(r_{13}+r_{33})/2$	T.6
	$r_{53}=-\frac{\sqrt{2}}{2}n_5^{-3}\left(\frac{\delta\Delta_{5\bar{5}5}}{t_{\bar{5}}E_5}+\frac{\delta\Delta_{\bar{5}5\bar{5}}}{t_5E_{\bar{5}}}\right)+n_5^{-3}(n_5-1)(d_{11}+d_{13}-d_{35})-(r_{11}+r_{31})/2$	T.7
Fig. 2(d)	$r_{61}=-\frac{\sqrt{2}}{2}n_6^{-3}\left(\frac{\delta\Delta_{6\bar{6}6}}{t_{\bar{6}}E_6}+\frac{\delta\Delta_{\bar{6}6\bar{6}}}{t_6E_{\bar{6}}}\right)+n_6^{-3}(n_6-1)(d_{22}+d_{21}-d_{16})-(r_{22}+r_{12})/2$	T.8
	$r_{62}=-\frac{\sqrt{2}}{2}n_6^{-3}\left(\frac{\delta\Delta_{6\bar{6}6}}{t_{\bar{6}}E_6}-\frac{\delta\Delta_{\bar{6}6\bar{6}}}{t_6E_{\bar{6}}}\right)+n_6^{-3}(n_6-1)(d_{11}+d_{12}-d_{26})-(r_{11}+r_{21})/2$	T.9

*For one-pass interferometers, e.g. Mach–Zehnder interferometer, all the values of $\delta\Delta_{ikl}$ in Tables 1–3 should be multiplied by factor 2.

4. Experimental determination of LEOE tensor components in $LiNbO_3$ and $LiNbO_3$:MgO crystals

The experimental technique presented above may be verified on electro-optic materials with known magnitudes of LEOE coefficients. One of such crystals is lithium niobate ($LiNbO_3$), extensively studied for electro-optic properties during the last several decades (see, e.g., Refs. [13,19]). In this section we present the experimental determination of static (mechanically "unclamped") LEOE tensor components of $LiNbO_3$ crystals and their doped modification $LiNbO_3$:MgO (7%). $LiNbO_3$ belongs to uniaxial crystals with the crystal structure described by the point group of symmetry 3m. Accordingly, the LEOE tensor consists of eight non-zero coefficients with only four independent coefficients, i.e. r_{22}, r_{13}, r_{33}, r_{51}. The four remaining ones are linearly related to them, i.e. $r_{12}=-r_{22}$, $r_{23}=r_{13}$, $r_{42}=r_{51}$ and $r_{61}=-r_{22}$ [12,14]. In order to determine their magnitudes it is sufficient to prepare three samples:

- The DC [i.e. the rectangular sample with faces that are perpendicular to the principal crystallophysical axes, see Fig. 2(a)] with the electrodes deposited on faces that are perpendicular to the X_2-axis. In order to determine the LEOE tensor coefficient r_{22}, light beam should be directed along the X_1- or X_3-axis and the light polarization must be set parallel to the X_2-axis.
- The DC [see Fig. 2(a)] with the electrodes deposited on faces that are perpendicular to the X_3-axis. In order to determine the LEOE tensor components r_{13} or r_{33}, light beam should be directed along the X_2-axis and light polarization must be set parallel to the X_1- or X_3-axis, respectively.
- The $X_2/45^{\circ}$-cut [see Fig. 2(c)] with electrodes deposited on faces that are perpendicular to the 5-axis (diagonal direction between X_1- and X_3-axes). In order to determine the LEOE tensor component r_{51}, light beam should be directed along the 5-axis and light polarization must be set parallel to the 5-axis.

In all cases we used gold electrodes that have been thermally deposited in vacuum. The set of samples mentioned above is minimally required to determine the four independent coefficients. For instance, additionally one may prepare the $X_1/45^{\circ}$-cut [see Fig. 2(b)] with electrodes deposited on faces that are perpendicular to the 4-axis. Such samples can be used for the direct measurement of the dependent LEOE tensor components r_{42}. In this case, light beam should be directed along the $\bar{4}$-axis and light polarization must be set parallel to the 4-axis. The magnitudes of linearly dependent tensor components r_{51} and r_{42} can be then compared to verify the interference technique used in this study.

The measurements have been done by means of the Michelson interferometer based on the half-wave voltage method in a static regime. Since according to this method $\delta\Delta_{ikl}=\lambda/2$ at $E_l=E_l^{\lambda/2}=U_l^{\lambda/2}/t_l$ (where $U_l^{\lambda/2}$ is the half-wave voltage) the corresponding equations take the following form:

$$r_{22}=-n_o^{-3}\frac{\lambda}{2E_2^{\lambda/2}t_1}+2n_o^{-3}d_{21}(n_o-1),$$

$$r_{33}=-n_e^{-3}\frac{\lambda}{2E_3^{\lambda/2}t_2}+2n_e^{-3}d_{32}(n_e-1),$$

Table 2
Reduced relations for determinations of the non-principal LEOE tensor components r_{il} in crystals of higher symmetry classes by means of Michelson interferometer

Crystal symmetry	Required samples	Reduced relation set	Equation
Monoclinic: 2	Figs. 2(a)–(d)	$r_{41}=-n_4^{-3}\dfrac{\delta\Delta_{4\bar{4}1}}{t_{\bar{4}}E_1}-n_4^{-3}(n_4-1)d_{14}$	T.10
		$r_{63}=-n_6^{-3}\dfrac{\delta\Delta_{6\bar{6}3}}{t_{\bar{6}}E_3}-n_6^{-3}(n_6-1)d_{36}$	T.11
		$r_{43}=-\sqrt{2}n_4^{-3}\dfrac{\delta\Delta_{4\bar{4}4}}{t_{\bar{4}}E_4}+n_4^{-3}(n_4-1)(d_{22}+d_{23}-d_{34})-(r_{22}+r_{32})/2$	T.12
		$r_{61}=-\sqrt{2}n_6^{-3}\dfrac{\delta\Delta_{6\bar{6}6}}{t_{\bar{6}}E_6}+n_6^{-3}(n_6-1)(d_{22}+d_{21}-d_{16})-(r_{22}+r_{12})/2$	T.13
Monoclinic: m	Figs. 2(a)–(d)	$r_{42}=-\sqrt{2}n_4^{-3}\dfrac{\delta\Delta_{4\bar{4}4}}{t_{\bar{4}}E_4}+n_4^{-3}(n_4-1)(d_{32}+d_{33}-d_{24})-(r_{23}+r_{33})/2$	T.14
		$r_{62}=-\sqrt{2}n_6^{-3}\dfrac{\delta\Delta_{6\bar{6}6}}{t_{\bar{6}}E_6}+n_6^{-3}(n_6-1)(d_{11}+d_{12}-d_{26})-(r_{11}+r_{21})/2$	T.15
Orthorhombic: 222	Figs. 2(b)–(d)	r_{41}—according to Eq. (T.10)	
		$r_{52}=-n_5^{-3}\dfrac{\delta\Delta_{5\bar{5}2}}{t_{\bar{5}}E_2}-n_5^{-3}(n_5-1)d_{25}$	T.16
		$r_{63}=-n_6^{-3}\dfrac{\delta\Delta_{6\bar{6}3}}{t_{\bar{6}}E_3}-n_6^{-3}(n_6-1)d_{36}$	T.17
Orthorhombic: mm2	Figs. 2(a)–(c)	$r_{51}=-\sqrt{2}n_5^{-3}\dfrac{\delta\Delta_{5\bar{5}5}}{t_{\bar{5}}E_5}+n_5^{-3}(n_5-1)(d_{31}+d_{33}-d_{15})-(r_{13}+r_{33})/2$	T.18
		r_{42}—according to Eq. (T.5)	
Trigonal: 3	Figs. 2(a)–(c)	r_{41} or r_{51}—according to Eqs. (T.1) or (T.18), respectively	
Trigonal: 32	Figs. 2(a, b)	r_{41}—according to Eq. (T.1)	
Tetragonal: 4 Hexagonal: 6	Figs. 2(a)–(c)	r_{41} and r_{51}—according to Eqs. (T.1) or (T.10) and (T.14) or (T.18), respectively	
Tetragonal: 422 Hexagonal: 622	Fig. 2(a) or (c)	r_{41}—according to Eqs. (T.1) or (T.10), respectively	
Trigonal: 3m Tetragonal: 4mm Hexagonal: 6mm	Fig. 2(a)–(c)	r_{42} or r_{51}—according to Eqs. (T.14) or (T.18), respectively	
Tetragonal: $\bar{4}2$m	Figs. 2(b)–(d)	r_{41}, r_{52} and r_{63}—according to Eqs. (T.10), (T.16) (T.17), respectively	
Cubic: 23, $\bar{4}3$m	Fig. 2(b)	r_{41}—according to Eqs. (T.1) or (T.10)	

$$r_{13}=-n_o^{-3}\frac{\lambda}{2E_3^{\lambda/2}t_2}+2n_o^{-3}d_{32}(n_o-1),$$
$$r_{51}=-\sqrt{2}n_5^{-3}\frac{\lambda}{2E_5^{\lambda/2}t_{\bar{5}}}+n_5^{-3}(n_5-1)(d_{31}+d_{33}-d_{15})-(r_{13}+r_{33})/2, \quad (10)$$

where $n_5=\sqrt{2}/\sqrt{n_o^{-2}+n_e^{-2}}$ with the ordinary n_o and extraordinary n_e refractive indices as derived for $LiNbO_3$ ($n_o=2.2865$; $n_e=2.2034$) and $LiNbO_3$:MgO ($n_o=2.2841$; $n_e=2.1994$) crystals by the interference-rotation technique [20,21]. The piezoelectric coefficients have also been determined by acoustic method and exhibit the following magnitudes (in the units of 10^{-12} C/N): $d_{22}=20.1$, $d_{31}=-0.57$, $d_{33}=6.9$, $d_{15}=66.6$ and $d_{22}=19.2$, $d_{31}=0.40$, $d_{33}=4.1$, $d_{15}=66.6$ for $LiNbO_3$ and $LiNbO_3$:MgO, respectively. The details regarding these studies will be published elsewhere. We have also performed the electro-optic measurements by a standard optical polarization technique by detecting the changes of phase retardation $\delta\Delta^*_{kl}=2\delta[(n_i-n_j)t_k]=2\delta[\Delta n_k\, t_k]$ (Δn_k is the optical birefringence) under the applied electric field. The LEOE coefficients r^*_{kl} have been calculated by means of the equation

$$r^*_{kl}=-\frac{\delta\Delta^*_{kl}}{U_l}\frac{t_l}{t_k}+2d_{lk}(n_i-n_j), \quad (11)$$

and then compared with LEOE coefficients $r^*_{kl}=r_{il}n_i^3-r_{jl}n_j^3$ as measured by the interferometry technique [14]. In some cases the LEOE coefficients r_{il} can be obtained directly from the optical polarization measurements. In particular, taking into account the relations

$$r_{22}=\tfrac{1}{2}r^*_{32}n_o^{-3} \quad \text{for } l=2,\ k=3, \quad (12)$$

or

$$r_{22}=-r^*_{12}n_o^{-3} \quad \text{for } l=2,\ k=1, \quad (13)$$

one may measure the tensor coefficient r_{22}. It should be stressed that the birefringence measurements (by using, e.g., Senarmonth compensator) are much simpler and reveal considerably better accuracy compared to the interferometric technique. For this reason such measurements are always preferred whenever this is possible.

One must have in mind that due to inverse piezoelectricity the measured LEOE coefficients may contain two contributions, i.e. the direct and indirect ones. The direct (or purely electro-optic) contribution is related to the changes of optical indicatrix under the applied electric field whereas the indirect (or electro-piezo-optic) contribution acts through the photoelastic effect caused by the piezoelectric deformation. Having the piezoelectric d_{lk} and photoelastic p_{ik} tensor components one may evaluate the

Table 3
Additional relations for the 45°-cut samples

Sample	Relations	Equation
Fig. 2(b)	$r_{11}=-n_1^{-3}\dfrac{\delta\Delta_{1\bar{4}1}}{t_{\bar{4}}E_1}+n_1^{-3}(n_1-1)(d_{12}+d_{13}-d_{14})$	T.18
	$r_{11}=-n_1^{-3}\dfrac{\delta\Delta_{141}}{t_4E_1}+n_1^{-3}(n_1-1)(d_{12}+d_{13}+d_{14})$	
	$r_{11}=-\dfrac{1}{2}n_1^{-3}\left(\dfrac{\delta\Delta_{1\bar{4}1}}{t_{\bar{4}}E_1}+\dfrac{\delta\Delta_{141}}{t_4E_1}\right)+n_1^{-3}(n_1-1)(d_{12}+d_{13})$	
Fig. 2(c)	$r_{22}=-n_2^{-3}\dfrac{\delta\Delta_{2\bar{5}2}}{t_{\bar{5}}E_2}+n_2^{-3}(n_2-1)(d_{21}+d_{23}-d_{25})$	T.19
	$r_{22}=-n_2^{-3}\dfrac{\delta\Delta_{252}}{t_5E_2}+n_2^{-3}(n_2-1)(d_{21}+d_{23}+d_{25})$	
	$r_{22}=-\dfrac{1}{2}n_2^{-3}\left(\dfrac{\delta\Delta_{2\bar{5}2}}{t_{\bar{5}}E_2}+\dfrac{\delta\Delta_{252}}{t_5E_2}\right)+n_2^{-3}(n_2-1)(d_{21}+d_{23})$	
Fig. 2(d)	$r_{33}=-n_3^{-3}\dfrac{\delta\Delta_{3\bar{6}3}}{t_{\bar{6}}E_3}+n_3^{-3}(n_3-1)(d_{31}+d_{32}-d_{36})$	T.20
	$r_{33}=-n_3^{-3}\dfrac{\delta\Delta_{363}}{t_6E_3}+n_3^{-3}(n_3-1)(d_{31}+d_{32}+d_{36})$	
	$r_{33}=-\dfrac{1}{2}n_3^{-3}\left(\dfrac{\delta\Delta_{3\bar{6}3}}{t_{\bar{6}}E_3}+\dfrac{\delta\Delta_{363}}{t_6E_3}\right)+n_3^{-3}(n_3-1)(d_{31}+d_{32})$	

mechanically "clamped" LEOE coefficient r_{il}^{u} [12]:

$$r_{il}^{u}=r_{il}^{\sigma}-\sum_{k=1}^{k=6}p_{ik}d_{lk}, \tag{14}$$

where r_{il}^{σ} are mechanically "unclamped" electro-optic coefficients (here $r_{il}^{\sigma}\equiv r_{il}$ according to our previous notations) and the second term describes the indirect piezoelectric contribution to the total electro-optic effect.

The results regarding the measurements of $LiNbO_3$ and $LiNbO_3$:MgO crystals are presented in Tables 4 and 5, respectively. Both tables specify the sample geometry that has been used in each measurement, the effective driving voltage U_{ef} defined as the

Table 6
Photoelastic coefficients of $LiNbO_3$ and $LiNbO_3$:MgO crystals as determined by the interferometric technique

	$LiNbO_3$	$LiNbO_3$:MgO
p_{11}	-0.021 ± 0.018	-0.015 ± 0.013
p_{12}	0.060 ± 0.019	0.058 ± 0.014
p_{13}	0.172 ± 0.029	0.174 ± 0.026
p_{31}	0.141 ± 0.017	0.155 ± 0.018
p_{33}	0.118 ± 0.020	0.154 ± 0.019
p_{14}	-0.052 ± 0.007	-0.044 ± 0.007
p_{41}	-0.109 ± 0.017	-0.149 ± 0.032
p_{44}	0.121 ± 0.019	0.136 ± 0.030
$\sum p_{in}$	0.794	0.884

Table 4
Results of the electro-optic measurements of $LiNbO_3$ crystals for various sample geometries

Interferometric measurements						Optical polarization measurements			
Sample geometry lki	Effective driving voltage U_{ef} (V)	Measured LEOE coefficients r_{il} (10^{-12} m/V)	Contribution of r_{il} into $\delta\Delta_{ikl}$ (%)	Contribution of d_{lk} into $\delta\Delta_{ikl}$ (%)	Evaluated data $r_{kl}^{*}=r_{il}n_i^3-r_{jl}n_j^3$ (10^{-12} m/V)	Effective driving voltage U_{ef} (V)	Measured coefficients r_{kl}^{*} (10^{-12} m/V)	Contribution of r_{kl}^{*} into $\delta\Delta_{kl}$ (%)	Contribution of d_{lk} into $\delta\Delta_{kl}$ (%)
232	3750	$r_{22}=6.7\pm0.4$	100	0	$r_{32}^{*}=167$	2020	$r_{32}^{*}=157\pm4\Rightarrow r_{22}=6.51\pm0.18$	100	0
231	3710	$r_{12}=-7.3\pm0.5$	100	0					
212	2350	$r_{22}=6.9\pm0.7$	61.6	38.4	$r_{12}^{*}=-83$	3570	$r_{12}^{*}=-85\pm2\Rightarrow r_{22}=7.09\pm0.12$	96	4
213	7160	$r_{32}=0\Rightarrow d_{21}=-18.3\pm0.5$	0	100					
323	840	$r_{33}=34.9\pm0.7$	99.6	0.4	$r_{23}^{*}=-247$	1390	$r_{23}^{*}=-228\pm9$	100	0
321	2440	$r_{13}=10.6\pm0.3$	98.8	1.2					
312	2730	$r_{23}=9.6\pm0.5$	98.7	1.3	$r_{13}^{*}=219$	1310	$r_{13}^{*}=241\pm26$	100	0
313	940	$r_{33}=31.5\pm0.4$	99.6	0.4					
$5\bar{5}5$	660	$r_{51}=30.1\pm1.3$	88.9	11.1					
$4\bar{4}4$	620	$r_{42}=32.1\pm2.3$	93.1	6.9					

Table 5
Results of the electro-optic measurements of $LiNbO_3$:MgO crystals for various sample geometries

Interferometric measurements						Optical polarization measurements			
Sample geometry lki	Effective driving voltage U_{ef} (V)	Measured LEOE coefficients r_{il} (10^{-12} m/V)	Contribution of r_{il} to $\delta\Delta_{ikl}$ (%)	Contribution of d_{lk} to $\delta\Delta_{ikl}$ (%)	Evaluated data $r_{kl}^{*}=r_{jl}n_j^3-r_{il}n_i^3$ (10^{-12} m/V)	Effective driving voltage U_{ef} (V)	Measured coefficients r_{kl}^{*} (10^{-12} m/V)	Contribution of r_{kl}^{*} to $\delta\Delta_{kl}$ (%)	Contribution of d_{lk} to $\delta\Delta_{kl}$ (%)
212	2310	$r_{22}=7.5\pm0.7$	64.1	35.9	-88 ± 8	3430	$r_{12}^{*}=-89\pm3\Rightarrow r_{22}=7.47\pm0.21$	96.5	3.5
321	2460	$r_{13}=10.7\pm0.3$	100.8	-0.8	-240 ± 9	1510	$r_{23}^{*}=-210\pm10$	100	0
323	870	$r_{33}=34.5\pm0.8$	100.3	-0.3					
312	2350	$r_{23}=11.1\pm0.5$	100.8	-0.8	232 ± 9	1560	$r_{13}^{*}=203\pm7$	100	0
313	910	$r_{33}=34.1\pm0.7$	100.3	-0.3					
$4\bar{4}4$	640	$r_{42}=34.9\pm1.3$	85.7	14.3					

Table 7
Summarized magnitudes of the mechanically "unclamped" r_{ij}^{σ} and mechanically "clamped" r_{ij}^{u} electro-optic coefficients (in 10^{-12} m/V) of $LiNbO_3$ and $LiNbO_3$:MgO crystals as summarized according to Tables 4 and 5 or taken from the literature for $LiNbO_3$ crystals

Crystal	r_{22}		r_{33}		r_{13}		r_{51}		Ref.
	r_{22}^{σ}	r_{22}^{u}	r_{33}^{σ}	r_{33}^{u}	r_{13}^{σ}	r_{13}^{u}	r_{51}^{σ}	r_{51}^{u}	
$LiNbO_3$	6.79±0.15	4.9	33.2±0.6	32.5	10.1±0.4	8.9	31.1±1.8	18.6	Our data
$LiNbO_3$	6.8	3.4	32.2	30.8	10	8.6	32	28.0	[19]
		3.95±0.2		30.6±3.5		7.8±0.5		28.2±0.5	[22]
	7	3	33	31	10	9	33	28	[23]
	6.81		30.9	30.8	9.6	8.6	32	18.2	[24]
	6.8		32.2	28.4	10	7.68	32.6	28	
	6.7		34		10.9		–		
$LiNbO_3$:MgO	7.47±0.21	5.9	34.3±0.8	33.5	10.9±0.4	10.2	34.9±1.3	20.1	Our data

half-wave voltage $U_l^{\lambda/2}$ for a sample with dimensions of $1\times1\times1$ cm^3, the magnitudes of the measured LEOE tensor components r_{kl} or r_{kl}^*, the percentage of the electro-optic (r_{il}) and piezoelectric (d_{lk}) contributions to the electro-induced optical path $\delta\Delta_{ikl}$ or phase retardation $\delta\Delta_{kl}^*$, and magnitudes of the coefficients r_{kl}^* as evaluated from interferometric measurements. The error in the determination of the LEOE coefficients has been evaluated by considering in each case the accuracy of piezo-optic and half-wave voltage measurements. They obviously have major influence on the error magnitude. On the other hand, the errors related to the crystal length or refractive index measurements have negligibly small influence on the total error value and for this reason they were ignored. The direct and indirect electro-optic contributions have been evaluated by using the photoelastic coefficients measured by the interferometric technique for both crystals [see Table 6]. The indirect contribution for most electro-optic coefficients is considerable, especially for r_{51} (40% and 43%) and r_{22} (28% and 21%), as for $LiNbO_3$ and $LiNbO_3$:MgO crystals, respectively, which may be explained by relatively large magnitudes of the corresponding piezoelectric coefficients.

The magnitudes of several LEOE tensor components obtained for various sample geometries, but expected to be equal, appear indeed to be slightly different, which may be explained by the limited accuracy of measurements as well as by possible inhomogeneity of the grown single crystals since the samples have been cut from different parts of the crystal. For this reason Table 7 summarizes the results regarding the electro-optic measurements of $LiNbO_3$ and $LiNbO_3$:MgO crystals, which are averages over different sample geometries used in the study. For comparison this table also contains data obtained by other authors for $LiNbO_3$ crystals. Comparing the tensor components for $LiNbO_3$ and $LiNbO_3$:MgO crystals one may conclude that the latter ones are characterized by somewhat higher magnitudes (statistically about 10%).

5. Conclusions

We have presented here a technique which is very suitable for determination of LEOE tensor components in crystal materials of any symmetry. The method is based on the Michelson interferometer, where the sample being studied is set into one of its arms to measure electro-induced changes of the optical path. The paper describes in detail the sample geometries that are needed to determine a complete set of LEOE tensor components and also derives the corresponding equations. The experimental technique has then been tested and verified on lithium niobate crystals, which represent a classic electro-optic material with well-known magnitudes of LEOE tensor components. It was applied to new crystals of MgO-doped $LiNbO_3$ as well to study their electro-optic properties. The measurements reveal that $LiNbO_3$:MgO crystals are characterized by magnitudes of LEOE tensor components that exceed in average about 10% of the corresponding magnitudes of pure $LiNbO_3$ crystals. This may be important for many applications, especially those dealing with powerful laser radiation. In the general case even pure $LiNbO_3$ single crystals are frequently characterized by intrinsic non-stoichiometric defects leading to substantial modifications of the electro-optic coefficients (see Ref. [25]). For this reason the developed method can be especially useful in optical engineering, which deals with crystal materials being directly used in design or production of electro-optic devices, such as, e.g., modulators or deflectors.

Acknowledgments

This work has been supported by STCU-program (Project no. 3222) and the Austrian FWF (Project no. P19284-N20).

References

[1] Voloshinov VB, Knyazev GA. Acoustooptic cells with nonuniform length of light–sound interaction. Tech Phys 2003;48:1475–9.
[2] Shuvalov LA, Urusovskaya AA, Zheludev IS. Physical properties of crystals, vol. 4. Berlin: Springer; 1988. p. 583.
[3] Bernal M-P, Roussey M, Baida FI. Near- and far-field verification of electro-optic effect enhancement on a tunable lithium niobate photonic crystal. J Microsc 2008;229:264–9.
[4] Rezzonico D, Jazbinsek M, Guarino A, Kwon O-P, Günter P. Electro-optic Charon polymeric microring modulators. Opt Express 2008;16:613–27.
[5] Garzarella A, Qadri SB, Wu DH, Hinton RJ. Responsivity optimization and stabilization in electro-optic field sensors. Appl Opt 2007;46:6636–40.
[6] Brosi J-M, Koos C, Andreani LC, Waldow M, Leuthold J, Freude W. High-speed low-voltage electro-optic modulator with a polymer-infiltrated silicon photonic crystal waveguide. Opt Express 2008;16:4177–91.
[7] Jacobsen RS, Andersen KN, Borel PI, Fage-Pedersen J, Frandsen LH, Hansen O, et al. Strained silicon as a new electro-optic material. Nature 2006;441:199–202.
[8] Andreev IA. Two decades following the discovery of thermally stable elastic properties of $La_3Ga_5SiO_{14}$ crystal and coining of the term "langasite" (a review). Tech Phys 2004;49:1101–3.
[9] Mytsyk BG, Andrushchak AS. Spatial distribution of the longitudinal and transverse piezooptical effect in lithium tantalate crystals. Crystallogr Rep 1996;41:1001–6.
[10] Andrushchak AS, Bobitski YaV, Kaidan MV, Mytsyk BG, Kityk AV, Schranz W. Two-fold interferometric measurements of piezo-optic coefficients: application to β-BaB_2O_4 crystals. Opt Laser Technol 2005;37:319–28.
[11] Kaidan MV, Tybinka BV, Zadorozhna AV, Schranz W, Sahraoui B, Andrushchak AS, et al. The indicative surfaces of the photoelastic effect in Cs_2HgCl_4 biaxial crystals. Opt Mater 2007;29:475–80.
[12] Narasimhamurty TS. Photoelastic and electro-optic properties of crystals. New York: Plenum; 1981. p. 514.

[13] Cook WR, Nelson DF, Vedam K. Piezooptic and electrooptic coefficients. Landolt-Börnstein series group III in condensed matter, vol. 30A. New York: Springer; 1996. p. 497.
[14] Sonin AS, Vasilevskaya AS. Electro-optic crystals. Moscow: Atomizdat; 1971. p. 327 [in Russian].
[15] Sugak DYu, Matkovskii AO, Solskii IM, et al. Growth and optical properties of $LiNbO_3$:MgO single crystals. Cryst Res Technol 1997;32:805–9.
[16] Andrushchak AS, Mytsyk BG, Demyanyshyn NM, Kaidan MV, Yurkevych OV, Kityk AV, et al. Spatial anisotropy of linear electro-optic effect for crystal materials: II. Indicative surfaces as efficient tool for electro-optic coupling optimization. Opt Lasers Eng, doi:10.1016/j.optlaseng.2008.08.007.
[17] Standards on piezoelectric crystals. Proc IRE 1949;37:1378–97.
[18] Mytsyk BG, Andrushchak AS. A positive directions choice of the crystallophysical axes in the piezooptical effect investigation. Ukr J Phys 1993;38:1015–21 [in Ukrainian].
[19] Grigoreva IS, Meylihova EZ, editors. Physical values: reference book. Moscow: Energoatomizdat; 1991. p. 1232. [in Russian].
[20] Andrushchak AS. Two-beam interferometer for refractive indices measurement of the isotropic and anisotropic materials. Patent no. 2102700, Russian Federation, 1998.
[21] Andrushchak AS, Tybinka BV, Ostrovskij IP, Schranz W, Kityk AV. Automated interferometric technique for express analysis of the refractive indices in isotropic and anisotropic optical materials. Opt Lasers Eng 2008;46:162–7.
[22] Kaminov JP, Jonston WJ. Quantitative determination of sources of the electrooptic effect in $LiNbO_3$ and $LiTaO_3$. Phys Rev 1967;160:519–22.
[23] Crystal Technology, Inc., an EPCOS company. Lithium niobate optical crystals. 〈www.crystaltechnology.com〉, p. 1–2.
[24] Nikogosyan DN. Properties of optical and laser-related materials. A handbook. Chichester–New York–Weinheim–Brisbane–Singapore–Toronto: Wiley; 1997. p. 594.
[25] Kityk IV, Makowska-Janusik M, Fontana MD, Aillerie M, Abdi F. Influence of non-stoichiometric defects on optical properties in $LiNbO_3$. Cryst Res Technol 2001;36:577–89.